Master of Science Thesis

Hybrid Eulerian-Lagrangian Vortex Particle Method

A fast and accurate numerical method for 2D Vertical-Axis Wind Turbine

L. Manickathan B.Sc.

Date TBD

Faculty of Aerospace Engineering · Delft University of Technology

TU Delft Delft University of Technology

Challenge the future

Hybrid Eulerian-Lagrangian Vortex Particle Method

A fast and accurate numerical method for 2D Vertical-Axis Wind Turbine

Master of Science Thesis

For obtaining the degree of Master of Science in Aerospace Engineering at Delft University of Technology

L. Manickathan B.Sc.

Date TBD

Faculty of Aerospace Engineering · Delft University of Technology

TU Delft Delft University of Technology

Delft University Of Technology
Department Of
Aerodynamics and Wind Energy

The undersigned hereby certify that they have read and recommend to the Faculty of Aerospace Engineering for acceptance a thesis entitled **"Hybrid Eulerian-Lagrangian Vortex Particle Method"** by **L. Manickathan B.Sc.** in partial fulfillment of the requirements for the degree of **Master of Science**.

Dated: Date TBD

Head of department:
prof.dr.ir. G.J.W. van Bussel

Academic Supervisor:
dr.ir. C.J. Simao Ferreira

Academic Supervisor:
dr.ir. A. Palha da Silva Clerigo

Industrial Supervisor:
prof.dr.ir. I. Bennett

Summary

This is the summary of the thesis.

Acknowledgements

I wish to thank the following persons…

Delft, The Netherlands
Date TBD

L. Manickathan B.Sc.

Contents

List of Figures

List of Tables

Nomenclature

Latin Symbols

c^2	Diffusion parameter	$[-]$
$\mathcal{E}$	Enstrophy	$[m^2 \cdot s^{-2}]$
h	Nominal particle spacing	$[m]$
h_ν	Characteristic diffusion distance	$[m]$
$\mathbf{K}$	Biot-Savart kernel	$[-]$
$\mathbf{K}_\sigma$	Vortex blob kernel	$[-]$
$\mathbf{A}$	Vortex panel influence matrix	$[-]$
k_d	Diffusion frequency multiple	$[-]$
$\hat{\mathbf{n}}$	Normal vector	$[-]$
N_p	Number of particles	$[-]$
overlap	Overlap ratio of the blobs	$[-]$
p	Pressure	[Pa]
$\hat{\mathbf{s}}$	Tangent vector	$[-]$
t	Time	$[s]$
$\mathbf{u}$	Velocity	$[m \cdot s^{-1}]$
$\mathbf{u}_b$	Velocity of the body	$[m \cdot s^{-1}]$
$\mathbf{u}_\gamma$	Vortex sheet induced velocity	$[m \cdot s^{-1}]$
$\mathbf{u}_{\text{ext}}$	External induced velocity	$[m \cdot s^{-1}]$
$\mathbf{u}^h$	Discrete velocity	$[m \cdot s^{-1}]$
u_θ	Angular velocity	$[m \cdot s^{-1}]$
$\mathbf{u}_\infty$	Free-stream velocity	$[m \cdot s^{-1}]$

$\mathbf{u}_\phi$	Potential velocity	$[m \cdot s^{-1}]$
u_r	Radial velocity	$[m \cdot s^{-1}]$
$\mathbf{u}_{\text{slip}}$	Boundary slip velocity	$[m \cdot s^{-1}]$
$\mathbf{u}_\omega$	Vortical velocity	$[m \cdot s^{-1}]$
W	Interpolation kernel weight	$[-]$
$\mathbf{x}$	Position vector	$[m]$
$\mathbf{x}_\nu$	Position vector of particle to be diffused	$[m]$
$\mathbf{x}_p$	Position vector of the particle	$[m]$

Greek Symbols

α_p	Circulation of the particle	$[m^2 \cdot s^{-1}]$
β_p	Corrected circulation of the particle	$[m^2 \cdot s^{-1}]$
Γ	Circulation	$[m^2 \cdot s^{-1}]$
Γ_b	Circulation of moving body	$[m^2 \cdot s^{-1}]$
γ	Vortex sheet strengths	$[s]$
Γ_γ	Circulation of vortex sheet	$[m^2 \cdot s^{-1}]$
Γ_ω	Circulation of the fluid	$[m^2 \cdot s^{-1}]$
Δt_c	Convection time-step size	$[s]$
Δt_d	Diffusion time-step size	$[s]$
ϵ	Relative error	$[-]$
ζ_σ	Smooth cut-off function of the blob	$[-]$
ν	Kinematic viscosity	$[m^2 \cdot s^{-1}]$
ξ	Scale relative position of particle to stencil node	$[-]$
ρ	Density	$[kg \cdot m^{-3}]$
σ	Core size	$[m]$
ω	Vorticity	$[s^{-1}]$
ω^h	Discrete vorticity field	$[s^{-1}]$

Abbreviations

CSVM	Constant-Strength Vortex Method
FMM	Fast-Multipole Method
GPU	Graphics Processing Units
LHS	Left Hand Side
LSTSQ	Least-Square solution method
PSE	Particle Strength Exchange

VAWT	Vertical-Axis Wind Turbine
VPM	Vortex Particle Method
VRM	Vortex Redistribution Method

Chapter 1

Introduction

Conventional energy resources such as fossil fuels and nuclear energy are not only limited supply but also pose adhere effects on the environment. Therefore, we are striving to find a cheap and renewable source of energy. Wind energy is such source of energy and is getting more popular, and have also become more affordable. Novel renewable technologies such as Vertical-Axis Wind turbines is now an interested research field.

Vertical-Axis Wind Turbine (VAWT) are unlike the normal wind turbine. Typical wind turbines are mounted on a mast away from the ground and generates energy by spinning normal to the ground. However, a VAWT spins parallel to the ground with its hub located at the ground [25]. The advantages of the vertical axis wind turbine are what makes them ideal for a source of renewable energy. As the turbine is located at the ground, it is easily accessible and can be easily maintained. The second main advantage of the VAWT is the way it dissipates its wake [9] [23]. As the fluid past the turbine is more turbulent, the flow is able to smooth out much earlier. This means that it possible to places VAWTs much closer to each other is so in future this means that a VAWT farm can potentially give more power per area. Furthermore, they operate independent of the flow direction, and can operate at low wind speeds (low tip-speed ratios).

However, with these advantages also comes some drawbacks. As the blades passes through its own dirty air (the wake), complex wake-body interactions take places. These have adhere effect on the blade structure and therefore is more susceptible to fatigue. This happens because the blades are constantly pitching, and complex flow behaviour such as dynamic stall and constant vortex shedding occurs [19]. This complex fluid behaviours makes it hard to predict the performance of a VAWT and this is one of the reasons why VAWTs are not mainstream. In addition, as the VAWT operates at large Reynolds number, accurate numerical methods are computationally very expensive. Therefore, it is vital to have a good understanding of the flow structure evolution and the wake generation of the VAWT using not only an efficient method, but also an accurate one.

1.1 Motivation and Goal

The goal of the research is to develop an efficient, reliable, and accurate numerical method for modelling the flow around a 2D VAWT such that one is able to deduce the correct performance characteristics of the VAWT. The two main approaches of investigate the flow is either using a numerical method to simulate the flow or by performing real-life experimental tests.

To understand the unsteady aerodynamic behaviour, Particle Image Velocimetry (PIV) has been as useful tool to visualize the flow around the turbine. Ferreira et al. (2007) [8], have shown that it was possible to acquire flow characteristics around the blade, and these method had the accuracy to be used as validation tools. However, the downside to experimental investigation is that is it very expensive to investigate all types of configuration. Furthermore, the model sizes are limited by the dimensions of the wind tunnel and investigations with arrays of VAWT is difficult.

Numerical methods are a popular alternative as the cost of simulation and the accuracy of the models are increasing day by day. In the research field, there exists many models with various orders of accuracy. Actuator Disk (AD) and Blade Element Momentum (BEM) models are one of simplest models that are build upon satisfying the momentum balance of the turbine and the fluid. The advantage of theses models are that they are very quick, however they lack the accuracy that can be achieved by experimental simulation. Complex blade-wake interactions such as dynamic stalls and flow separations cannot be modeled by these methods.

To ensure more accuracy, one has to solve the Navier-Stokes equation of the flow around the turbine. Compuational Fluid Dynamic (CFD) methods discretizes the fluid into smaller regions and solves the set of Navier-Stokes equation in each region (or grids). This type of formulation is known as an Eulerian method as we are evaluating the change in flow property of a given region. In order to fully resolve the flow around the turbine, we would have to discretize the fluid at the order of the size of the vortex cores. As the vortex cores are very small (a fraction of size of the airfoil) near the blade, and very large far away from the blade (in order of size of the turbine), we must have grid size that adapts. This requires a large number of grids, as the blades are constantly moving, and makes it computation very expensive to solve especially for arrays of turbines.

An alternative method is to use the vortex formulation of the Navier-Stokes equations, referred to as vorticity equation. This method is ideal because when describing it in Lagrangian formulation, the vorticity evolution is evaluated as interaction between vortices, and this removes the requirement of gridding. In addition, using simulation acceleration methods such as Fast Multipole Method (FMM) and parallel computation in Graphical Processing Units (GPU), they are much more efficient that typical CFD methods and can easily be scaled to distributed computation. However, vortex method cannot inherently take in account the solid body. They require additional methods that can describe the effect of the body in the fluid and the vorticity generated from the body.

So, we see that Eulerian method is accurate when describing the blade-wake interaction but are not efficient when describing multi-scale domains. Whereas, the Lagrangian method is very efficient in evolution the vorticity of the fluid, and is an ideal choice when describing the multi-scale flow characteristics. Therefore, in order to use the advantage of both methods, we have decided to use a domain-decomposition method, referred to as Hybrid Eulerian-Lagrangian Vortex Particle Method (HVM). In this method, the Eulerian formulation will be used at the region around the blade and Lagrangian formulation will be used everywhere else. With proper coupling of these methods, we can ensure that the this numerical method can capturing not only the near-wake phenomenons such as vortex shedding, dynamic stall, and the wake-body interaction, but also the capture the large-scale flow structures such as the evolution of the VAWT wake, with efficiency and accuracy.

1.2 Research Aim and Plan

Research Question: *Is it possible to develop an efficient and accurate numerical method by an hybrid approach where the vortex particle method is used in the wake, and the Navier-Stokes grid solver is used at the near-body region? Will it be able to simulate real life performance characteristics of a vertical axis wind turbine? Will it be able to predict similar performance characteristics and flow phenomena as observed from the wind tunnel experimental setup? Will it be capable of simulating the blade-wake interaction and the dynamic stall? Where are the errors and what are their sources?*

Research aim and plan:

- Develop the Hybrid method for capturing small-scale phenomenons and large scale phenomenons.
- Ensure this tool is efficient, reliable, and accurate.
- Verify, Validate the tools with model problems.
- Apply the model to the 2D flow of VAWT.

In order to answer this research questions, the goal of the project is the develop an efficient and accurate numerical method that is not only capable of capture the small scale flow phenomena such as the dynamic stall and the vortex shedding, but is also efficient at modelling the wake evolution of VAWT. The investiga- tion will be performed for 2D geometries and the accuracy of the model needs to established first at simpler problems before continuing to more complex problem cases.

In other words, the initial goal is to develop the hybrid vortex particle method and verify the approach. During this process, the solver will be verified and validated against test cases starting from simpler prob- lems and gradually developing more complex features.

The final goal is to perform a simulation of a VAWT in 2D, compute its performance and validating it against experimental data. By the gradual development of the complex elements of the simulation, one can investigate the feasibility of such approach. Also, the investigation is only done for 2D currently as a full 3D simulation might be difficult and might not be feasible for the master thesis yet.

The innovativeness of this project is that such hybrid modeling has not been yet applied for the wind energy problem case. Through the parallelization of the vortex particle method in a GPU and employing solver acceleration techniques such as the FMM, this simulation could give an edge in the understanding the flow behaviour of a VAWT.

1.3 Introduction to Hybrid Eulerian-Lagrangian Vortex Particle Method

The Hybrid Eulerian-Lagrangian Vortex Particle Method (HVM) is a domain-decomposition method, where the Eulerian method and the Lagrangian method solves different domains of the fluid. The domain decomposition method is simply splitting the domain of interest and using the appropriate methods in each domain. For the problem of VAWT, as the boundary is non-trivial and is the source of vorticity, the full Navier-Stokes model will be used here, and away from the body where only the convection of the vorticity field is interested, the fast and efficient vortex particle method will be used, figure 1.1.

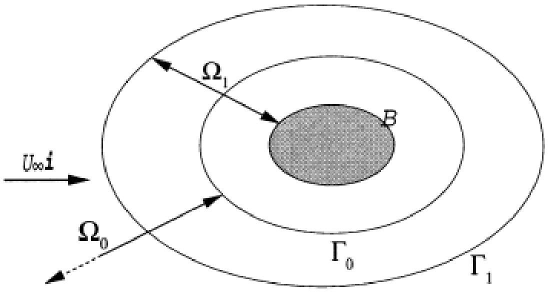

Figure 1.1: Domain decomposition: Navier-Stokes (near boundary), Vortex Particle Method (away from boundary), Guermond (2000) [10]

.

Several researches have already been done: Cottet and Koumoutsakos (2000a)[5], Guermond and Lu (2000) [10] simulating the advection dominated flows, Ould-Salhi et al. (2001) [16] blending finite difference and vortex method together, Winckelmans et al. (2005a) [27] investigating the trailing vorticies, Daeninck (2006) [6] implementing RANS and LES to the simulation, Stock (2010) [21] using GPU clusters for efficiency and Speck (2011) [20] implementing researching on multipole expansion and modified interpolation kernels.

As seen above, not all domain decomposition methods are the same. The main difference differencing between the methods is their coupling strategies. Most works employ the Schwartz alternating method to couple the vortex particle method and the grid solver. The Schwartz alternating method solve the grid solver initially and couples it with the vortex method by iteratively trying to satisfy the boundary conditions. However, for this project the coupling techniques that will be used is similar to Daeninck (2006) [6] and Stock (2010) [21], figure 1.2.

This new approach is much simpler and only a single iteration is needed for the coupling. The procedure is as follows: Solve the vortex method in the whole domain using relatively coarse evaluation, then use the grid solver in the near wall region to capture the detailed

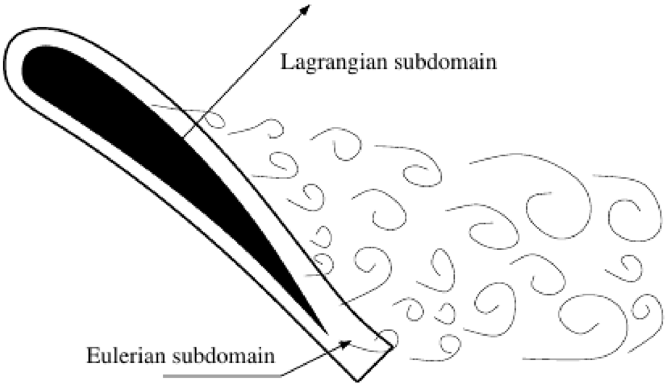

Figure 1.2: Modified domain decomposition: Without Schwartz Alternating method [6]

features of the boundary layer and translate the vorticity field at this region to the vortex particles. The functionality of this strategy has been demonstrated by Daeninck and was found to be significantly faster than the Schwartz coupling strategy.

1.3.1 Advantage of domain decomposition

The advantage of the domain decomposition is that we can choose the method that should be used for the given domain.

-

1.4 Verification and Validation test case

The test-cases that are used for this thesis are given below:

- Lamb-Oseen Vortex
- Clercx-Bruneau dipole
- Impulsively started cylinder
- Elliptic Airfoil

1.4.1 Lamb-Oseen Vortex

To validate the vortex particle method, the Lamb-Oseen test case will be used. The vortex particle used blobs that carry the approximate the vorticity field. These blobs are then convected and diffused using the Biot-Savart Law [5], and are diffused using appropriate diffusion models [24]. The Lamb-Oseen test case is a standard benchmark case for validating the vortex method and it deals with the diffusion of the viscous vorticity field [17] [20] [?].

The Lamb-Oseen vortex model is given as

$$u_\theta = \frac{\Gamma}{2\pi r}\left[1 - \exp\left(-\frac{r^2}{4\nu t}\right)\right], \tag{1.1}$$

where u_θ is the circumferencial velocity and the radial velocity u_r is zero. The viscous core radius model is one of the simplest diffusion model and is ideal in validating the implemented diffusion model [?].

1.4.2 Clercx-Bruneau dipole

1.4.3 Impuslively Started Cylinder

he experimental set-up for coupled case is impulsively started cylinder. The cylinder is submerged into unpertubated flow and the vorticity evolution is investigated to validate the numerical method. Similar investigations have been done by Cheng et al. (1997) [?], Guermond and Lu (2000) [10], Issam and Ghoniem (2009) [?] and Rossinelli et al. (2010a) [?]. Again, these results will be used to validate the results of the coupled model, figure 1.3.

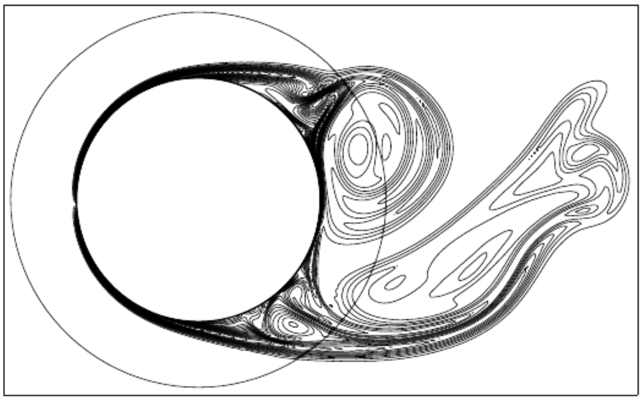

Figure 1.3: Vorticity contours of an impulsively started cylinder: Near-wall (Navier-Stokes), away-wall (Vortex Method) dipole-wall collsion [6]

1.5 Methodology

The initial steps of the development of the hybrid vortex methods is as follows:

- Develop the vortex particle method
- Validate the vortex particle method against a Lamb-Oseen convection test case.

- Develop the vortex panel method to deal with the boundaries for the vortex particle calculation.
- Validate the vortex panel method by solving a potential flow around a cylinder.
- Develop the grid solver that is based on the Finite Element method.
- Validate the grid solver against test cases: impulsively starting cylinder, dipole-Wall interaction.

Once all the components have been validated, the methods will be coupled and validated against similar test cases.

- Couple vortex particle, vortex panel and grid solver together.
- Validate it with the previous generated test case solution.
- Introduce more complicated phenomenons: multiple geometry (i.e multiple grid meshes) and moving boundaries, if it feasible in the constraints of a master thesis.

If the coupled solver has been validated with the test cases, the final step will be to simulated the flow around a VAWT and investigating the performance vs. numerical and experimental data.

1.6 Thesis Outline

Chapter 2

Lagrangian Domain: Vortex Particle Method

2.1 Introduction to Vortex Particle Method

Vortex Particle Method (VPM) is a branch of computational fluid dynamics that deals with the evolution of the vorticity of the fluid in a lagrangian description. Typically, the fluid is viewed at a fixed window where it is described as a function of space **x** and time t. However, the lagrangian point of view regards the fluid as a collection of the particles carrying the property of the fluid.

Unlike the typical eulerian method that require discretization of all the fluid domain, VPM only needs fluid elements where there is vorticity. This means that the VPM are inherently auto-adaptive method that only simulated the flow of interest. Furthermore, with the computational acceleration methods such as Fast-Multipole Method (FMM) and parallel computation on Graphics Processing Units (GPU), VPM can be more efficient that typical eulerian methods.

2.1.1 Vorticity

Vorticity ω, the governing element of vortex particle method, is defined as

$$\omega = \Delta \times \mathbf{u}, \tag{2.1}$$

where **u** is the velocity. The circulation Γ is defined as

$$\Gamma = \int_L \mathbf{u} \cdot d\mathbf{r} = \int_S \omega \cdot \mathbf{n} \; dS, \tag{2.2}$$

by the stokes theorem, as represents the integral vorticity of the domain, figure 2.1

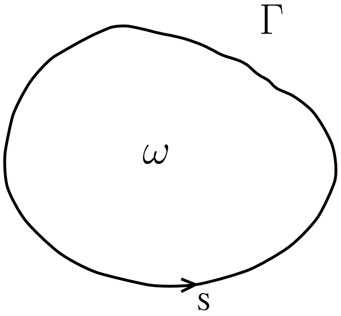

Figure 2.1: Circulation of the fluid

2.1.2 Velocity-vorticity formulation of the Navier-Stokes equations

The governing equation of the vortex particle method is velocity-vorticity $\mathbf{u}-\omega$ formulation of the Navier-Stokes equations [5]. The 2-D incompressible Navier-Stokes momentum equation is given as

$$\frac{\partial \mathbf{u}}{\partial t}+\mathbf{u}\cdot\nabla\mathbf{u}=-\frac{1}{\rho}\nabla p+\nu\nabla^2\mathbf{u}, \tag{2.3}$$

relating the velocity field $\mathbf{u}\left(\mathbf{x},t\right)$ to the pressure field $\mathbf{p}\left(\mathbf{x},\mathbf{t}\right)$, the kinematic viscosity ν and density ρ. Furthermore, we also have to satisfy the incompressibility constraint given as

$$\nabla\cdot\mathbf{u}=0. \tag{2.4}$$

To attain the velocity-vorticity formulation, we should take the curl of the velocity-pressure $\mathbf{u}-p$ formulation of the Navier-Stokes equation. Taking the curl of the momentum equation 2.3, we get the vorticity transport equation

$$\frac{\partial \omega}{\partial t}+\mathbf{u}\cdot\nabla\omega=\nu\nabla^2\omega, \tag{2.5}$$

which only relates the vorticity to the velocity enabling us to neglect the pressure field. Note that as we are dealing with the two dimensional flow, we neglected the stretching term.

2.1.3 Viscous splitting algorithm

Vortex particle method was initially used to model the evolution of incompressible, inviscid flows. However, in order to simulate a real flow, we must also deal with the viscous behaviour of the fluid. Chorin [3] has shown that using the viscous splitting algorithm, it is possible to simulate a viscous flow.

The viscous splitting algorithm is basically a fractional step method, where the viscous and the inviscid part of the transport equation is dealt in two subsequent steps,

- Sub-step 1: convection
$$\frac{\partial \omega}{\partial t} + \mathbf{u} \cdot \nabla \omega = 0; \tag{2.6}$$
- Sub-step 2: diffusion
$$\frac{\partial \omega}{\partial t} = \nu \nabla^2 \omega. \tag{2.7}$$

The first sub-step of the evolution deals with the convection of the vorticity. Note that, by convection we imply the advection of the vorticity field where the diffusion process is neglected. The second sub-step is where we deals with the diffusion of the vorticity field.

There are several advantage to this type of evolution. As the convection and diffusion are handled separately, there is minimum dispersion during the convection and furthermore, the is no restriction of the advection CFL number [24].

There are many ways of dealing with the diffusion of the vorticity field. During this project, we use a modified interpolation kernel [24] that can simultaneously treat diffusion and remesh the vortex particles, see section 2.3.

2.2 Spatial Discretization: Generation of Vortex Blobs

In order to deal with the vorticity field, we must first discretize the vorticity to vortex particles. Vortex blobs have been first introduced by Chorin and is a mollified particle carrying the local circulation. Vortex blobs describes a smooth vorticity field and are ideal because of it does not cause singularity issues when particles approach each other.

!!! check for consistency, continuity !!!

2.2.1 Biot-Savart law

The velocity field can be decomposed using the Helmholtz decomposition, given as

$$\mathbf{u} = \mathbf{u}_\omega + \mathbf{u}_\phi, \tag{2.8}$$

where $\mathbf{u}_\omega$ is the rotational component of the velocity and $\mathbf{u}_\phi$ is the irrotational component. solenoidal and potential velocity respectively. In an unbounded flow we have $\mathbf{u}_\phi$ equal to the free-stream velocity $\mathbf{u}_\infty$. For bounded flow, we must include the presence of the body, see section 2.4.

The velocity can be related to the vorticity using the Biot-Savart law

$$\mathbf{u}_\omega = \mathbf{K} \star \omega, \tag{2.9}$$

where the $\star$ represents convolution of the 2-D kernel $\mathbf{K}$ given by

$$\mathbf{K} = \frac{1}{2\pi \left|\mathbf{x}\right|^2} \left(-x_2, x_1\right). \tag{2.10}$$

2.2.2 Discrete form of vorticity field

The spatial discretization of the fluid domain is done through N quadrature points. With the Biot-Savart law, we can treat these quadratures are discrete particles carrying the local quantities. The discrete vorticity field is given as

$$\omega\left(\mathbf{x},t\right)\simeq\omega^{h}\left(\mathbf{x},t\right)=\sum_{p}\alpha_{p}\left(t\right)\delta\left[\mathbf{x}-\mathbf{x}_{p}\left(t\right)\right], \tag{2.11}$$

where α_p is the estimate of the circulation around the particle $\mathbf{x}_p$ with core size σ. We must not that ω^h is an approximately equal to ω of the fluid due to the discretization.

The discrete form of the velocity is therefore written as

$$\mathbf{u}\simeq\mathbf{u}^{h}=\sum_{p}\mathbf{K}\left[\mathbf{x}-\mathbf{x}_{p}\left(t\right)\right]\alpha_{p}\left(t\right). \tag{2.12}$$

Thus the discrete vorticity field is an N-body problem inducing velocity on each and implicitly evolving the vorticity field. This is one of the advantage of the vortex particle method as there are many ways to efficiently treat the problem. The N-body problem can be parallelized and can be accelerated using fast summation methods such as FMM, see **??**.

However, like all N-body problem, equation 2.10 has a singularity when the particles approach each other and can result in numerical instability. To overcome this we can mollify the kernel, removing the singularity.

2.2.3 Convection of vortex blobs

In the discrete of the convection equation 2.6 of the viscous-splitting algorithm, the is solved as system of ODEs, where

$$\frac{\mathrm{d}\mathbf{x}_p}{\mathrm{d}t}=\mathbf{u}\left(\mathbf{x}_p\right), \tag{2.13}$$

with

$$\frac{\mathrm{d}\alpha_p}{\mathrm{d}t}=0. \tag{2.14}$$

As the diffusion is done at the next sub-step, we have to ensure that the circulation is conserved.

2.2.4 Mollified vortex kernels

A vortex particle with a mollified core, non-zero core-size, is referred to as vortex blobs. The advantage of the vortex blobs is that the with a smooth distribution of the vorticity, the singularity disappears and so numerical instability does not happen when blobs get too close to each other. An ideal choice for a cutoff function is a Gaussian distribution, figure 2.2.

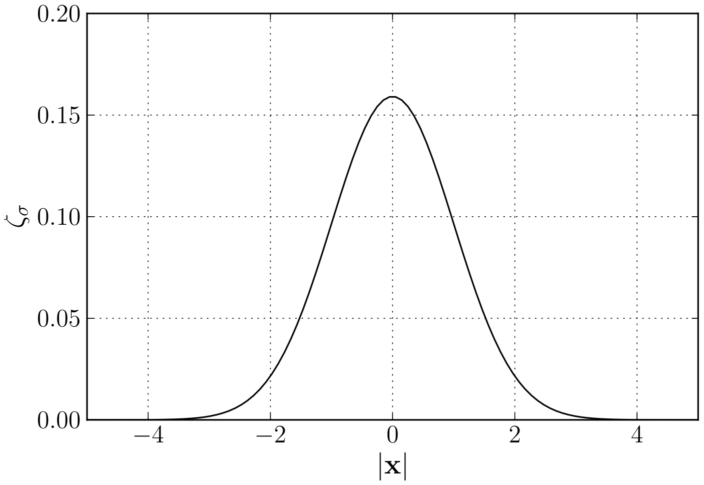

Figure 2.2: Vortex blob with Gaussian distribution: $[k = 2,\ \sigma = 1.0]$

Gaussian kernels satisfy the requirement for smooth distribution ad decays quickly and is defined as

$$\zeta_\sigma = \frac{1}{k\pi\sigma^2} \exp\left(\frac{-|\mathbf{x}|}{k\sigma^2}\right), \tag{2.15}$$

where k is 1, 2 or 4 and determines the width of the kernel, σ is core-size of the blob. Note that smoothing function is chosen such that $\int \zeta = 1$, ensuring the conservation of circulation when mollified. So, using a smooth cut-off function ζ_σ, the mollified kernel $\mathbf{K}_\sigma$ is given as

$$\mathbf{K}_\sigma = \mathbf{K} \star \zeta_\sigma. \tag{2.16}$$

The mollified vorticity field, represented by vortex blobs is given as

$$\omega^h(\mathbf{x}, t) = \sum_p \alpha_p(t)\, \zeta_\sigma\left[\mathbf{x} - \mathbf{x}_p(t)\right], \tag{2.17}$$

now representing the mollified vorticity field and equivalently, the mollified velocity field is given as

$$\mathbf{u}^h(\mathbf{x}, t) = \sum_p \mathbf{K}_\sigma\left[\mathbf{x} - \mathbf{x}_p(t)\right] \alpha_p(t). \tag{2.18}$$

Koumoutsakos and Chorin [5], have shown that for proper communication between the particle, the particle needs to overlap,

$$\text{overlap} = \frac{\sigma}{h}, \tag{2.19}$$

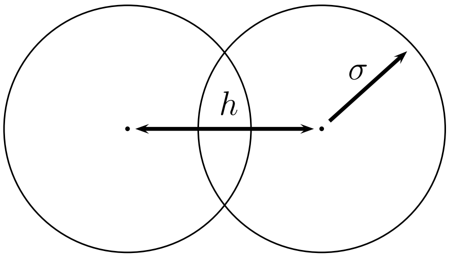

Figure 2.3: Vortex blob with overlap σ/h

where h is the nominal particle spacing, figure 2.3. If the particles fail to overlap, vortex blobs will also fail to recover the vorticity field. Such problems occurs when blobs are clustered due to high flow strain, leading to lagrangian grid distorting and must be treated, see section 2.2.6.

2.2.5 Vortex blob initialization

Now the question arises on how to initialize the particle's circulation strengths α_p. A common approach that is used is to estimate the particles strength is to say that

$$\alpha_p = \omega_p \cdot h^2. \tag{2.20}$$

This might seem like a valid assumption as the circulation of a given area is the integral of the vorticity in the area, equation 2.2, however this is no longer valid when regularizing the vorticity field using mollified gaussian kernels, equation 2.17. Barba and Rossi [1], has described this problem as gaussian blurring of the original vorticity field. Even though the particle have acquired the correct circulation strengths (i.e the local property), when evaluating the mollified vorticity field, we see that there is a mismatch in the evaluated vorticity field, figure 2.4.

Another way of viewing this characteristic is say the conservation of circulation is only valid globally, but not locally. A common standard for recovering the initial vorticity field is perform the Beale's method [2].

Beale's Iterative Method

The Beale's method is particle circulation processing scheme where the circulation of the particles are modified such that the mollified vorticity field matches the indented vorticity field. The recovery of the vorticity field is done by performing a discrete deconvolution,

$$\sum_{j}^{N} \beta_j \zeta_\sigma \left(\mathbf{x}_i - \mathbf{x}_j\right) = \omega_i, \tag{2.21}$$

where β_j is the circulation of the particles at positions $\mathbf{x}_j$ such that it matches the exact vorticity ω_i at the position $\mathbf{x}_i$ that we are evaluating. As we are try to solve for a N

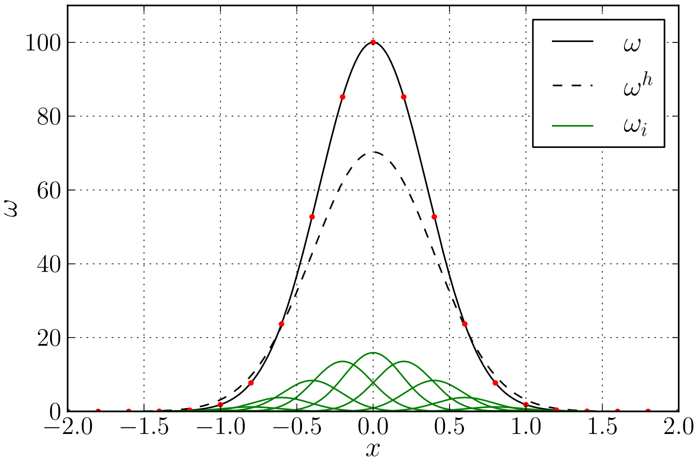

Figure 2.4: Mollified vorticity field of an arbitrary vorticity function with $\text{overlap} = 1.0$, $\sigma = 0.19$, $h = 0.19$. Vortex blob strength has assigned by equation 2.20, sampling at exact vorticity [●, red dot]. Figure depicts exact vorticity distribution ω [—, solid], vorticity field of each blob ω_i [—, green dashed], the mollified vorticity field ω^h [- -, dashed].

unknown problem, we must set up a N system of equations. Multiplying both sides with the area associated to the blobs, we get

$$\mathbf{A}_{ij}\beta_j = \alpha_i^{\text{exact}}, \tag{2.22}$$

where

$$\mathbf{A}_{ij} = \zeta_\sigma\left(\mathbf{x}_i - \mathbf{x}_j\right) \cdot h^2 \tag{2.23}$$

is a $N \times N$ matrix containing the weights of the influence of each particle on each other. This matrix can be constructed by setting the Γ to one and determine the induced vorticity on each other. Furthermore, we see that it is not feasible to directly invert the matrix when we have large set of blobs but most importantly as the matrix $\mathbf{A}$ is severly ill-conditioned [20], it should not be directly inverted. Beale's proposition to this problem was to iteratively solve for the solution,

$$\beta_j^{n+1} = \alpha_i + \beta_i^n - \mathbf{A}_{ij} \cdot \beta_j^n \tag{2.24}$$

We see that with just two iterations, the error between the mollified and exact vorticity field reduces drastically, figure 2.5. Koumoutsakos and Cottet [5], had shown that there was a drastic improvement in the velocity with just two to three iterations. However, we see that the cell vorticity of the blobs, directly evaluated from the particle strengths, equation 2.20, are more peaky and no longer matches the exact vorticity.

During the hybrid coupling algorithm, we see that this is the central source of coupling error between the eulerian and the lagrangian method, section **??**. When performing the hybrid coupling, we need to recover the vorticity field transfered from the eulerian domain

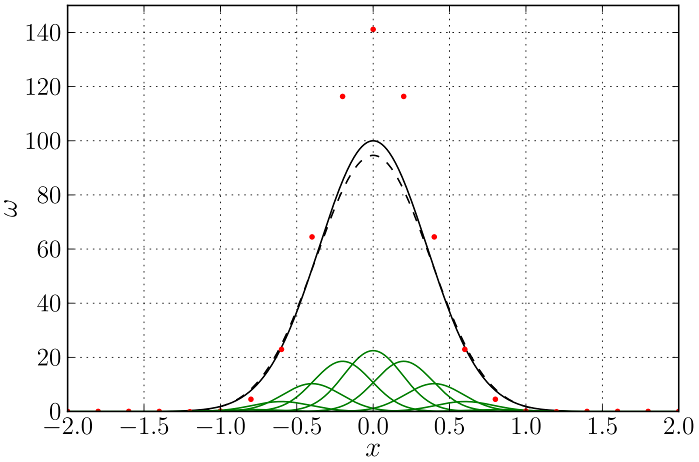

Figure 2.5: Mollified vorticity field after two Beale's iteration, overlap $= 1.0$, $\sigma = 0.19$, $h = 0.19$. Figure depicts exact vorticity distribution ω [—, solid], vorticity field of each blob ω_i [—, green dashed], the mollified vorticity field ω^h [- -, dashed].

to the lagrangian domain in every step. So, beale's correction is not a viable solution for the hybrid method. Thus there is a need for an alternate method of recovering the vorticity field.

!!! add the reference to hybrid !!!

Convergence of particle discretization

An alternate, temporary method to reduce the gaussian blurring of the vorticity field is to reduce the overlap (i.e. increase the overlap ratio) of the vortex blobs and to the increase the spatial resolution.

Figure 2.6 shows mollified vorticity field results from modifying the spatial resolution parameters. Figure 2.6a shows the convergence of the mollified vorticity field ω^h to

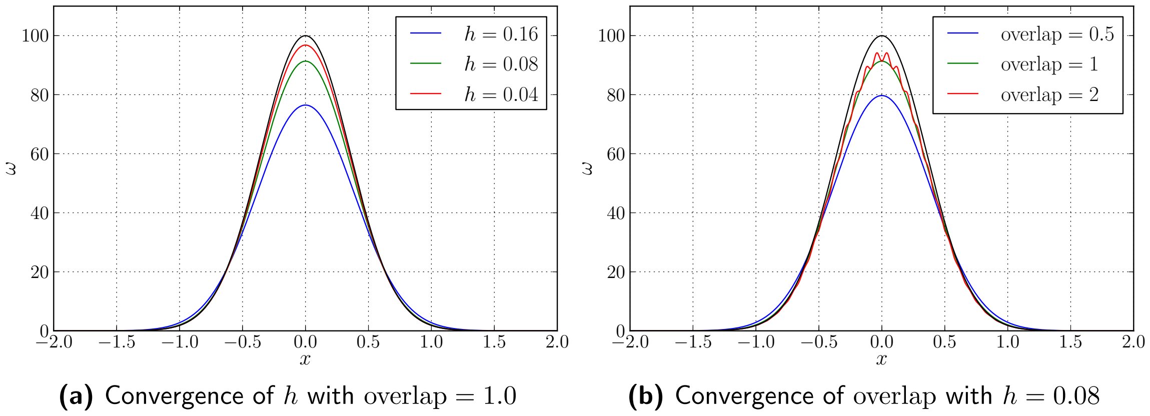

(a) Convergence of h with overlap $= 1.0$

(b) Convergence of overlap with $h = 0.08$

Figure 2.6: Convergence of vorticity by modifying the spatial resolution. Figure depicts exact vorticity field ω with [—, black] and various resolutions.

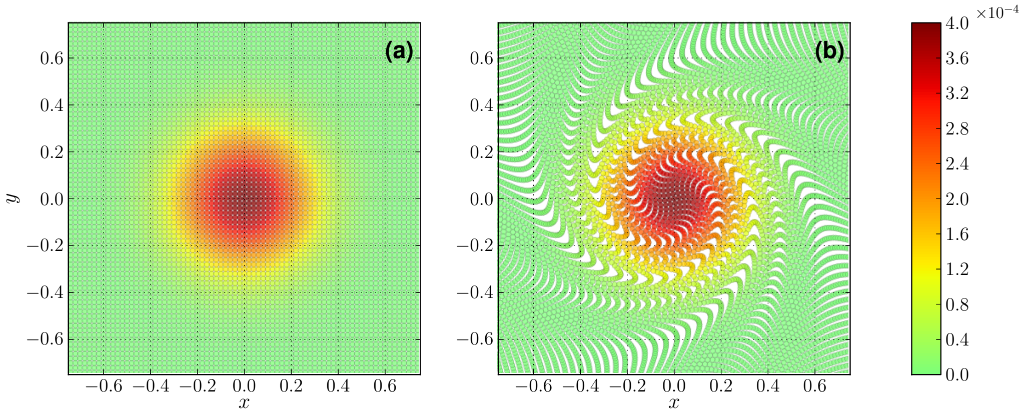

Figure 2.7: Lagrangian distortion of the vortex blobs after 100 steps. The initial vorticity field $\omega(\mathbf{x},0) = \exp(-12|\mathbf{x}|)$ with $\Delta t = 0.1$, $\sigma = 0.02$ and $\text{overlap} = 1.0$. Figure depicts **(a)** the initial and **(b)** the final distribution of the vortex blobs.

the exact vorticity field ω by reducing the nominal particle spacing h. The blobs have overlap $= 1$ and so the blob core-size σ is equal to h. We see that as you reduce the size of the blob and increase the number of particles, the mollified vorticity converges to the exact vorticity. Therefore, an alternate method of reducing the gaussian blurring is to increase the spatial resolution.

Furthermore, we could also adjust the overlap of the blobs, figure 2.6b. The σ and h of the blob is 0.08 and we see that increasing overlap number (i.e reducing the overlap), helps us to recover the original vorticity field. However, as explained by Koumoutsakos [5], if the overlap is too low, we lose the smooth recovery of the vorticity field. This is apparent when overlap $= 2.0$, where we see that the mollified vorticity field is fluctuation.

Therefore, for the hybrid coupling, we set overlap $= 1.0$ and maximize the spatial resolution at the coupling zone.

2.2.6 Remeshing scheme: Treating lagrangian grid distortion

During the convection step, we see that another source of error in the vorticity field is the lagrangian grid distortion. As we have seen before, when the vortex blobs fails to overlap, we are no longer able to reconstruct the correct the vorticity field, figure 2.6b. During the convection, due to the high strains in the fluid, the vortex blobs tent to clump together and creates regions where no vortex blobs are found, reducing the overlap of the blobs, figure 2.7.

We see that due to clustering of the vortex blobs, it fails to reproduce the correct vorticity field. A common strategy to overcome this problem is to remesh the vortex blobs to a uniform grid, so that we have a continuous vorticity field.

However, when transfering the vorticity from the old deformed grid to the new lagrangian uniform grid, we must satisfy the conservation laws of vorticity field. The interpolation methods is based on the conservation of linear impulse which directly implies the

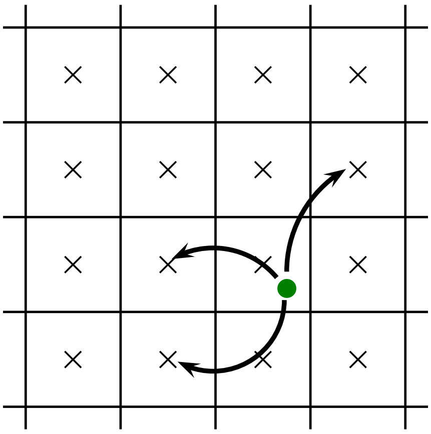

Figure 2.8: Remehsing of vortex blob (●, green) on the uniform grid defined by the (4×4) 2-D stencil.

conservation of the total circulation [5]. The transfer of the particle strengths is given as,

$$\alpha_p = \sum_q \tilde{\alpha}_q W \left(\frac{x_p - \tilde{x}_q}{h} \right), \tag{2.25}$$

where the strengths of the particles $\tilde{\alpha}_q$ of the distorted lagrangian grid $\tilde{x}_q$ is transfered to the regular lagrangian grid x_p using the interpolation kernel, weighted W, giving us the remeshing particle strengths α_p. The transfer of strengths of one particles to it's interpolation nodes can be seen in figure 2.8.

M_4' interpolation kernel

For lagrangian problem, we use the efficient interpolation kernel that has been used to reconstruct a smooth distribution interpolation, the M_4' interpolation kernel, introduced by Monaghan [15]. In one dimension it is given as,

$$\mathrm{M'}_4(\xi) = \begin{cases} 1 - \frac{5\xi^2}{2} + \frac{3|\xi|^3}{2} & |\xi| < 1, \\ \frac{1}{2}(2 - |\xi|)^2 (1 - |\xi|) & 1 \leq |\xi| < 2, \\ 0 & 2 \leq |\xi|, \end{cases} \tag{2.26}$$

where

$$\xi = \frac{x_\nu - x_i}{h} \tag{2.27}$$

is the scale relative position of the particle x_ν to the i^{th} interpolation node x_i. The $\mathrm{M'}_4$ is a third-order accurate piecewise smooth B-spline kernel, where $m = 4$ giving it 4 support nodes, figure 2.9. For the two dimensional problem that we have, the 2-D interpolation formula is simply tensor product of the 1-D interpolation kernel equation 2.26, and results in $4^2 = 16$ support nodes, figure 2.8.

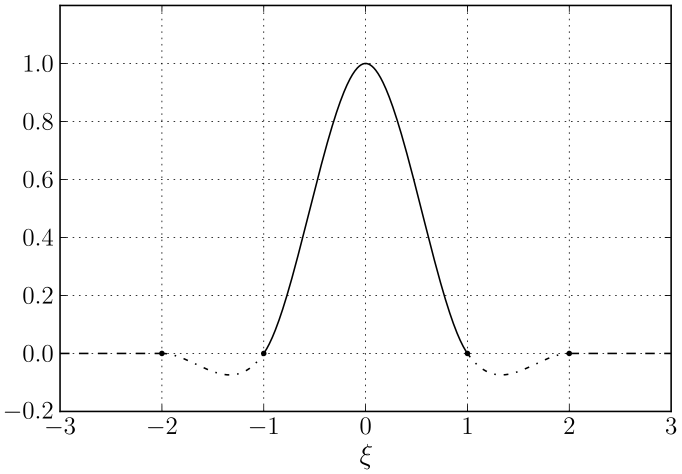

Figure 2.9: Monaghan's [15] third-order peicewise smooth B-spline kernel, M_4'

The interpolation kernel achieves the third-order accuracy as it also conserves the linear and the angular momentum of the vortex. Koumoutsakos [12] has investigated the drawback of the employing the remeshing strategy and have shown that there is approximately 4% decay in enstrophy of the flow due to sub-grid dissipation. Note that enstrophy $\mathcal{E}$, is defined as

$$\mathcal{E} = \frac{1}{2}\int_S \omega^2 dS \tag{2.28}$$

and is directly related to the kinetic energy of the fluid and gives and insight in the energy production and the dissipation of the fluid. Enstrophy is especially useful in turbulence flow investigation as it helps describe the energy cascade of the fluid.

2.3 Diffusion of Vortex Methods

So far, we have dealth with unbounded Euler flow, where we disregarded the viscosity of the flow. However, for real flow we must take in account of the diffusion of the vorticity. Chorin's approach to deal with the viscous term was to employ the viscous splitting algorithm. The flow is segregated to inviscid and viscous component and during the second sub-step we deal with the diffusion of the vorticity, equation 2.7. The equation can again be solved as a system of ODEs, similar to the convection step, where we say,

$$\frac{\mathrm{d}\mathbf{x}_p}{\mathrm{d}t} = 0, \tag{2.29}$$

with

$$\frac{\mathrm{d}\alpha_p}{\mathrm{d}t} = \nu\Delta\alpha_p. \tag{2.30}$$

Therefore in the diffusive step, we fix the position of the vortex blobs and only have to modify the strengths of the particles to mimic the diffusion process. Chorin initially employed a random walk method, which generates and disperse vorticity using pseudo-random number algorithm [3]. However, this method suffers some limitations in accuracy. Since then Particle Strength Exchange (PSE) method [7], has been a common approach that has been used to treat diffusion.

Particle Strength Exchange

The Particle Strength Exchange method, first proposed by Mas-Gallic [7], showed that diffusion can be treated for a particle method isotropic and anisotropic viscosity by approximating the diffusion operator (laplacian) with an integral operator and discretizing the operator using particles. The PSE can be seen as circulation correction method, where during the diffusion step of the viscous splitting algorithm, the strengths of the particle are corrected such that it accounts for the diffusion.

Vortex Redistribution Method

An alternative method to simulate the diffusion is to use the Vortex Redistribution Method (VRM) [17]. The model simulates diffusion by distributing the fraction of circulation of the vortex blobs to each other satisfying the diffusion. The model is based on conserving the moments of the particles by satisfying a linear system of equations. The circulation of the particle are transfer to the nearby particles that are

$$h_\nu = \sqrt{\nu \Delta t_d} \tag{2.31}$$

where h_ν is the diffusion distance and is directly related to the kinematic viscosity ν and the diffusive time-step Δt_d of the simulation. Not that the diffusive time-step Δt_d is equal to the convective time-step Δt_c if the diffusion process is done during every time-step. However, we can easily adjust the diffusion time-step and perform diffusion at a multiple step of the convection.

This is vital as a VRM (and also the PSE) requires a search algorithm to determine the particles that are within the zone of influence. A direct evaluation required $\mathcal{O}\left(N^2\right)$ evaluation, however can be speed up to $\mathcal{O}\left(\log N\right)$ using search tree algorithm.

The downside of the this approach, as also for the standard remeshing approach is the global remeshing generates large computation data and scales with the number of particles N. Therefore for problems with large number of particles, a tree-structured remeshing would be more feasible strategy [26].

2.3.1 Modified remeshing for treating diffusion

From further investigation of the VRM, we see that it is similar to remeshing strategy used to counter the lagrangian distortion during the convection process. Therefore Ghoniem and Wee [24] has proposed to combine the remeshing and the diffusion. The application of this methodology was validated by Speck [20]. The diffusion is simulated by the modifying the interpolation kernel of the remeshing process. The key advantage of the modified remeshing method is that now it deals with the uniform remeshing grid helping us eliminating the computational expensive research requirement. The second advantage as shown by the authors is the simplicity. The method only requires a slight modification to the original remeshing tool.

During remeshing, the heat equation is satisfied by transferring the correct fraction of circulation to produce the proper amount of diffusion. The $\mathrm{M'}_4$ kernel was modified to treat the diffusion and is given by:

$$\mathrm{M'}_4\left(\xi, c\right) = \begin{cases} 1 - \frac{5\xi^2}{2} + \frac{3|\xi|^3}{2} - c^2\left(2 - 9\xi^2 + 6|\xi|^3\right) & |\xi| < 1, \\ \frac{1}{2}(2 - |\xi|)^2\left(1 - |\xi|\right) - c^2(2 - |\xi|)^2\left(1 - 2\left|\xi\right|\right) & 1 \leq |\xi| < 2, \\ 0 & 2 \leq \left|\xi\right|, \end{cases} \tag{2.32}$$

where

$$c^2 = \frac{\nu \Delta t_d}{h^2}, \tag{2.33}$$

and corresponds to the transfer quantity for diffusion. The addition terms in the interpolation kernel accounts for the diffusion process. When $c \to 0$, the interpolation kernel turns to the classical non-diffusion kernel.

Similar to the VRM, we can perform the remeshing at a given multiple step k_d of the convection step. However, we have an additional constraint on the diffusion time-step Δt_d, equation 2.33. Wee and Ghoniem [24] also investigated the error growth and the stability properties of the interpolation kernel in the Fourier space and have determined that for $\mathrm{M'}_4$ interpolation kernel, we must satisfy

$$\frac{1}{6} \leq c^2 \leq \frac{1}{2}. \tag{2.34}$$

to ensure amplification factor and the phase error does not grow. This will ensure the stability of the problem and will suppress any spurious oscillations and ensure that it is a non-negative interpolation kernel with non-negative redistribution fractions.

However, we see that constraint on c^2 not only imposes a maximum Δt_d but also a constraint on the minimum Δt_d. This means that in scenarios, the $\Delta t_d = k_d \cdot \Delta t_c$ and this might introduce sudden change in vorticity field. Therefore, during the coupling of the lagrangian and eulerian domains, we would like to diffuse the vorticity after every convection scheme.

Simple redistribution scheme

The simple redistribution scheme based on the Shankar and Van Dommelen [17], developed by Tutty [22], makes it possible to remesh and diffuse the vorticity after every convection step,

$$\alpha_i^{n+1} = \sum_k \alpha_k^n W_{ki}^n, \tag{2.35}$$

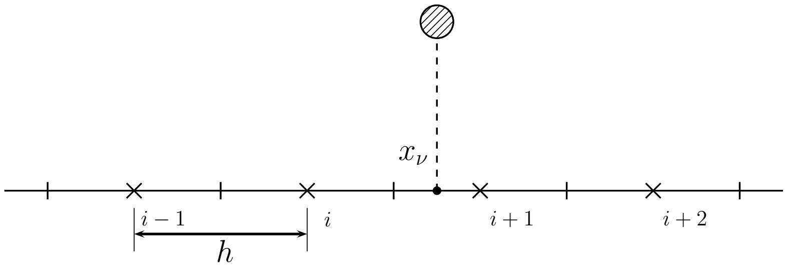

Figure 2.10: One dimensional, Simple redistribution scheme, diffusing the vortex blobs to the four stencil points ($k = i-1, \ldots, i+2$) with vortex blob positioned at $x_i \leq x_\nu \leq x_{i+1}$ and nominal blob spacing h.

where W^n_{ki} is the fraction of circulation from vortex blob k transferred to vortex blob i by diffusion during the time step n. The fractions W^n_{ki} are calculated by conserving vorticity, center of vorticity, linear, and angular momentum of the vortex blobs [22]. In two dimensional problem the redistribution fractions are simple tensors products of the x, y one dimensional redistribution fractions,

$$W_{kl} = F_k G_l, \quad k = i-1, \cdots, i+2, \quad l = j-1, \ldots, j+2 \tag{2.36}$$

giving it a 16 point stencil. The one-dimension redistribution fractions for x-direction is a linear combination of the two basis solution of the redistribution equation for conservations,

$$F_k = (1-\Delta) \cdot f_k + \Delta \cdot g_k, \quad k = i-1, \ldots, i+2 \tag{2.37}$$

having a four point stencil, figure 2.10. The basis solution of redistribution are

$$f_i = 1 - 2\left(\frac{h_\nu}{h}\right)^2 - \xi^2 \tag{2.38a}$$

$$f_{i-1} = \frac{1}{2}\left(1 - f_i - \xi\right) \tag{2.38b}$$

$$f_{i+1} = \frac{1}{2}\left(1 - f_i + \xi\right) \tag{2.38c}$$

and

$$g_{i+1} = 1 - 2\left(\frac{h_\nu}{h}\right)^2 - \xi_1^2 \tag{2.39a}$$

$$g_i = \frac{1}{2}\left(1 - g_{i+1} - \xi_1\right) \tag{2.39b}$$

$$g_{i+2} = \frac{1}{2}\left(1 - g_{i+1} + \xi_1\right) \tag{2.39c}$$

where ξ is given by equation 2.27, $\xi_1 = \xi - 1$ are the distances between the k^{th} stencil nodes x_k and the vortex blob that is to be diffused with $x_i \leq x_\nu \leq x_{i+1}$. Note, f_k and

g_k is zero for all the other k. In the above equation, h_ν is the characteristic diffusion distance over the time Δt_d,

$$h_\nu = \sqrt{\Delta t_d \cdot \nu}. \tag{2.40}$$

The only constraint imposed for positive redistribution fraction is

$$\frac{h_\nu}{h} < \frac{1}{\sqrt{2}}. \tag{2.41}$$

giving us the maximum time-step size constraint of

$$\Delta t_d < \frac{h^2}{2\nu}. \tag{2.42}$$

So now, we are able to perform diffusion, together with the convection step (i.e $k_d = 1$).

2.4 Boundary conditions at solid boundary

So far, we have only dealt with unbounded flow. During bounded flow simulation, we must impose addition constraint of the boundary to the simulation to simulate any flow about a geometry. From Helmholtz decomposition, we can have decompose the velocity field to the rotation and the irrotation component, equation 2.8. With the Helmholtz decomposition, we can use the potential component to prescribe the boundary conditions at the solid wall boundary,

$$\mathbf{u}_\phi = \nabla\Phi. \tag{2.43}$$

The incompressibility constraint results in a Laplace's equation for the potential field and unique solution is obtained by enforcing the wall boundary conditions,

$$\mathbf{u}_b \cdot \hat{\mathbf{n}} = (\mathbf{u}_\omega + \nabla\Phi) \cdot \hat{\mathbf{n}}, \tag{2.44}$$

and is defined as enforcing the no-through flow at the solid boundary wall, moving at $\mathbf{u}_b$. Note that the $\hat{\mathbf{n}}$ is the normal vector of the solid boundary. A classical approach for determine the solution to the Laplace's equation is by Green's function formulation. This approach required a singularity distribution over the body resulting in the appropriate boundary condition. Doublets and/or source panels are used to attain the required potential such that equation 2.44 is satisfied.

Linked boundary conditions

However Koumoutsakos, Leonard and Pepin [13], have suggested to enforce the boundary conditions through vortex sheets. The alternative approach of enforcing the solid boundary condition is not to decompose the velocity field into potential and rotational but to consider the solid boundary as an extension of the vorticity field through vortex sheets γ, figure 2.11. Due to the non-zero tangential velocity at the surface, a sudden

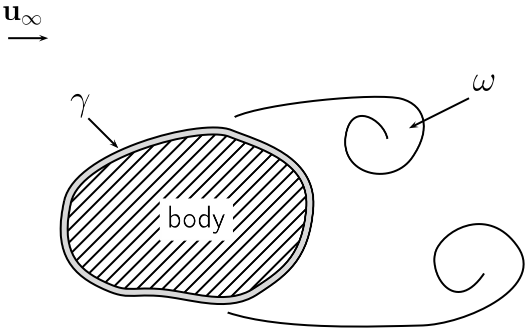

Figure 2.11: Extended vorticity field consisting of vorticity in the fluid and vortex sheet distribution around the body.

discontinuity in the velocity field can be considered as vortex sheet. Therefore, now to enforce the boundary conditions of the solid wall, we must satisfy the no slip velocity at the boundary,

$$\mathbf{u} \cdot \hat{\mathbf{s}} = \mathbf{u}_b \cdot \hat{\mathbf{s}}. \tag{2.45}$$

Koumoutsakos [14] only relies on the vortex sheet to enforce the no-slip velocity as no-slip boundary condition directly satisfies the no-through boundary conditions, also known as the linked boundary conditions. This was also proven by Shiels [18] and further investigated by Cooper, Mar and Barba [4] and shown that vortex sheet is the only necessary singularity element required to satisfy both the boundary conditions. Therefore, enforcing the no-slip boundary condition directly satisfies the no-through constraint at the surface.

2.4.1 Boundary integral equations

Thus the decomposed velocity field can be summarized as

$$\mathbf{u} = \mathbf{u}_\omega + \mathbf{u}_\gamma + \mathbf{u}_\infty \tag{2.46}$$

where the $\mathbf{u}_\gamma$ denotes the velocity filed induced by the vortex sheet. Applying the no-slip boundary conditions, we can say that

$$(\mathbf{u}_{\text{ext}} + \mathbf{u}_\gamma) \cdot \hat{\mathbf{s}} = \mathbf{u}_b \cdot \hat{\mathbf{s}} \tag{2.47}$$

where $\mathbf{u}_{\text{ext}} = \mathbf{u}_\omega + \mathbf{u}_\infty$ is the velocity field induced from domain external of the body and the vortex sheet. For the tangential boundary condition, for a well-conditioned system of equations, the induced velocity from the vortex sheet can be summarized as

$$(\mathbf{u}_{\text{ext}} - \mathbf{u}_b) \cdot \hat{\mathbf{s}} = \mathbf{u}_\gamma \cdot \hat{\mathbf{s}}. \tag{2.48}$$

The equation states that underneath the vortex sheet, we must have a vortex sheet inducing the velocity field $\mathbf{u}_\gamma$ to counter the slip velocity $\mathbf{u}_{\text{slip}} = (\mathbf{u}_{\text{ext}} - \mathbf{u}_b)$ such that we satisfy the no-slip kinematic boundary conditions. Note that, $\mathbf{u}_\gamma$ of equation 2.48, is negative of equation 2.47 as we looking under the vortex sheet. Koumoutsakos [14], expressed the

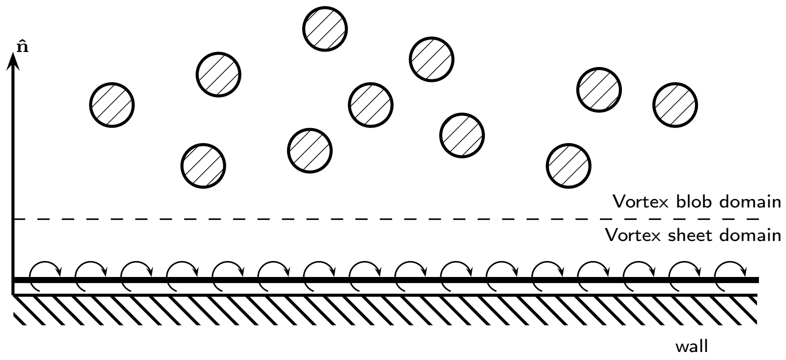

Figure 2.12: Extended vorticity field: Vortex sheet being an extension to the vorticity field (resolved by the vortex blobs) which is able to fully resolve the boundary vorticity

relation of the vortex sheet strengths to the no-slip boundary condition at the surface of the body (inside the body) through the Fredholm integral equation of the second kind,

$$-\frac{\gamma\left(s\right)}{2}+\frac{1}{2\pi}\oint\frac{\partial}{\partial n}\left[\log\left|\mathbf{x}\left(s\right)-\mathbf{x}\left(s'\right)\right|\right]\gamma\left(s'\right)ds'=\mathbf{u}_{\text{slip}}\cdot\hat{\mathbf{s}}. \tag{2.49}$$

The Left Hand Side (LHS) of the equation states at the point s, the velocity discontinuity is due to the vortex sheet at the point and the induced velocity of all the other vortex sheet acting on the point.

However, the equation 2.49 is not unique and accepts arbitrary solution for the vortex sheet strengths, therefore we must imposed an additional constraint on the strength of the vortex sheet. The addition constraint is a constraint on the net circulation of the vortex sheet. As the vortex sheet is considered as an extension to the vorticity field, we could say that the net circulation of the vortex panels is the circulation that was not captured by the vortex blobs, figure 2.12. As vortex blobs are not available very-near the body, it is not possible for the vortex blobs to resolve the high gradient vorticity at the boundary. Therefore, all the vorticity in the vortex sheet domain must be captured by the vortex sheet.

When considering a moving boundary, we must also take into account of the circulation of the body due to its motion. The net circulation of the problem is given as

$$\Gamma=\Gamma_{\omega}+\Gamma_{\gamma}+\Gamma_{b}=0, \tag{2.50}$$

where Γ_{ω} is the circulation of the vorticity in the fluid (i.e. the vortex blobs), Γ_{γ} is the wall bounded circulation (i.e. vortex sheets),

$$\Gamma_{\gamma}=\oint\limits_{S}\gamma\left(s\right)\ ds, \tag{2.51}$$

and the Γ_b is the circulation of the moving body. The circulation inside the body can be considered also be considered as an extension to the vorticity field, where the body is filled with uniform vorticity due to the rotation of the body. Therefore the circulation of a moving body can calculated simply integrating the “vorticity” inside the body

$$\Gamma_b = \iint\limits_{body} \nabla \times \mathbf{u}_b \, dA. \tag{2.52}$$

So the constraint imposed on the net circulation of the vortex sheets is given as,

$$\Gamma_\gamma = -\left(\Gamma_\omega + \Gamma_b\right). \tag{2.53}$$

Now, in a pure lagrangian, we must transfer the vorticity generated from the body to the fluid. This is typically done by diffusing the vorticity of the vortex on the fluid, however in our hybrid coupling method, we can use the eulerian domain to introduce the vorticity into the fluid. The eulerian domain acts as the near-wall solver [6], and the strengths of the particles is interpolated from the eulerian domain, section **??**. !!! CiTe Hybrid sectin !!!

2.4.2 Panel method for treating no-slip boundary condition

Equation 2.49 is solved by discretizing the body into M vortex panels giving us a system of equation with can used to determine the M unknowns of the strength of the vortex panels. The method refered as panel method has been greatly summarized by Katz and Plotkin [11].

Katz and Plotkins have shown several types of panel distributions with various orders of accuracy, from 0^{th} order point vortex or up to 2^{nd} order varying panel strength curvatured distribution. For this project, we have used a constant-strength vortex distribution that discretized the vortex sheet into straight segments, classified as Constant-Strength Vortex Method (CSVM).

Panel methods are constructed by discretizing the integral equation and forming a system of equations to solve the M unknowns of the vortex panel,

$$\underbrace{\begin{pmatrix} -\frac{1}{2} & a_{12} & \cdots & a_{1M} \\ a_{21} & -\frac{1}{2} & \cdots & a_{2M} \\ \vdots & \vdots & \ddots & \vdots \\ a_{M1} & a_{M2} & \cdots & -\frac{1}{2} \end{pmatrix}}_{\mathbf{A}_{MM}} \underbrace{\begin{pmatrix} \gamma_1 \\ \gamma_2 \\ \vdots \\ \gamma_M \end{pmatrix}}_{\vec{\gamma}} = \underbrace{\begin{pmatrix} \text{RHS}_1 \\ \text{RHS}_2 \\ \vdots \\ \text{RHS}_M \end{pmatrix}}_{\overrightarrow{\text{RHS}}} \tag{2.54}$$

where A_{MM} contains the weights of the influence of the vortex panels $\vec{\gamma}$ on each other and the $\overrightarrow{\text{RHS}}$ is

$$\text{RHS} = \mathbf{u}_{\text{slip}} \cdot \hat{\mathbf{s}} \tag{2.55}$$

is the boundary condition to the system of equations. In addition, we have another constraint on the net circulation of the vortex panels and in discrete from we say that,

$$\sum_{i}^{M} \gamma_i \Delta s = \Gamma_\gamma \tag{2.56}$$

and results in a $M+1$ system of equations for solving the M unknown strengths of the vortex panels,

$$\underbrace{\begin{pmatrix} -\frac{1}{2} & a_{12} & \cdots & a_{1M} \\ a_{21} & -\frac{1}{2} & \cdots & a_{2M} \\ \vdots & \vdots & \ddots & \vdots \\ a_{M1} & a_{M2} & \cdots & -\frac{1}{2} \\ \Delta s_1 & \Delta s_2 & \cdots & \Delta s_M \end{pmatrix}}_{\mathbf{B}_{(M+1)M}} \underbrace{\begin{pmatrix} \gamma_1 \\ \gamma_2 \\ \vdots \\ \gamma_M \end{pmatrix}}_{\vec{\gamma}} = \underbrace{\begin{pmatrix} \mathrm{RHS}_1 \\ \mathrm{RHS}_2 \\ \vdots \\ \mathrm{RHS}_M \\ \Gamma_\gamma \end{pmatrix}}_{\overrightarrow{\mathrm{RHS}}} \tag{2.57}$$

However, as we have an additional constraint on the net strength of the panels, we have $M+1$ set of equations with M unknowns giving us a overdetermined problem. The approach to solve such a problem is either by using a Least-Square solution method (LSTSQ), or introducing a new unknown or as used by Katz, eliminating an equation. Enforcing the no-slip boundary condition at each panel location is our vital criteria and therefore, elimination of an equation is not a viable strategy and so the LSTSQ method was utilized for the project.

Constant-Strength Vortex Method

The Constant-Strength vortex method (CSVM) is based on the flat (straight) discretization of the vortex sheet, where the panel have constant vortex strength as per definition. To solve the strengths of the panel problem, we enforce the dirichlet velocity boundary conditions at the collocation point x_{cp}, which is located just below the vortex sheet, figure 2.13b. The coefficient a_{ij} of the influence matrix $\mathbf{A}$ is defined as

$$a_{ij} = \hat{\mathbf{u}}_{ij} \cdot \hat{\mathbf{t}}_i, \tag{2.58}$$

and is the tangential influence coefficient of j^{th} panel on the i^{th} panel. Therefore, induced velocity $\hat{\mathbf{u}}_{ij} = (\hat{u}, \hat{v})_{ij}$ is the unit induced velocity of the j^{th} panel on to the collocation points of i^{th} panel, where the vortex panels have unit strength (i.e $\hat{\gamma}_i = 1$). In general, the induced velocity of the vortex panels are calculated in the local panel coordinates, figure 2.13, and the transformation from the local panel coordinate (x', y') to the global coordinates systems (x, y) is given by

$$\begin{bmatrix} u_{ij} \\ v_{ij} \end{bmatrix} = \begin{bmatrix} \cos\alpha_j & \sin\alpha_j \\ -\sin\alpha_j & \cos\alpha_j \end{bmatrix} \cdot \begin{bmatrix} u'_{ij} \\ v'_{ij} \end{bmatrix} \tag{2.59}$$

The induced velocity of the vortex panel j on the collocation point i is given as

$$u'_{ij} = \frac{\gamma_j}{2\pi}\left[\tan^{-1}\frac{y'_i - y'_{j,2}}{x'_i - x'_{j,2}} - \tan^{-1}\frac{y'_i - y'_{j,1}}{x'_i - x'_{j,1}}\right], \tag{2.60a}$$

$$v'_{ij} = -\frac{\gamma_j}{4\pi}\ln\frac{\left(x'_i - x'_{j,1}\right)^2 + \left(y'_i - y'_{j,1}\right)^2}{\left(x'_i - x'_{j,2}\right)^2 + \left(y'_i - y'_{j,2}\right)^2} \tag{2.60b}$$

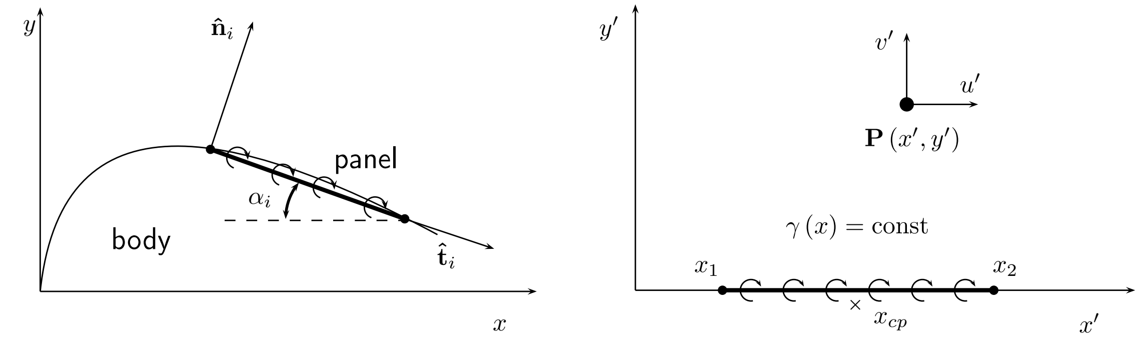

(a) Panel discretization of the body in the global cartesian coordinates system (x, y) and local panel coordinates rotated by α_i.

(b) Constant strength vortex panel in the local panel coordinate system (x', y') inducing velocity on the point P.

Figure 2.13: Vortex panel's global **(a)** and local **(b)** coordinates system definition as defined by Katz and Plotkins [11].

where $(x'_1, y'_1)_j$ and $(x'_2, y'_2)_j$ are the coordinates of the panel start and end point in its local panel coordinate system. Note that the self-induction of the vortex panel (when $i = j$), the influence coefficient becomes $a_{ij} = -1/2$, and can be seen in the diagonal terms of equation 2.54. So, by taking $\hat{\gamma}_i = 1$, we are able to construct the influence coefficients of the influence matrix $\mathbf{A}$ and can solve the strengths of the panel,

$$\mathbf{B} \cdot \gamma = \mathrm{RHS}, \tag{2.61}$$

using the LSTSQ method.

If we are dealing with multiple geometries, figure 2.14, the panel method can be easily

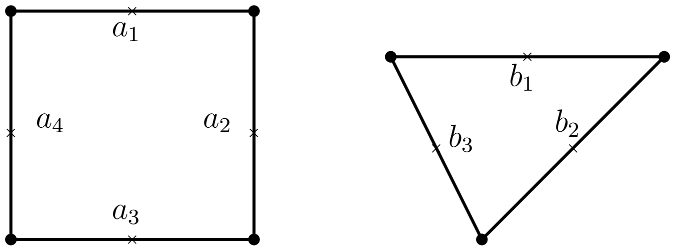

Figure 2.14: twoPanelBodies

extended by constructing a global influence matrix,

$$\underbrace{\begin{pmatrix} c_{a_1a_1} & \cdots & c_{a_1a_N} & c_{a_1b_1} & \cdots & c_{a_1b_M} \\ \vdots & \ddots & \vdots & \vdots & \ddots & \vdots \\ c_{a_Na_1} & \cdots & c_{a_Na_N} & c_{a_Nb_1} & \cdots & c_{a_Nb_M} \\ c_{b_1a_1} & \cdots & c_{b_1a_N} & c_{b_1b_1} & \cdots & c_{b_1b_M} \\ \vdots & \ddots & \vdots & \vdots & \ddots & \vdots \\ c_{b_Ma_1} & \cdots & c_{b_Ma_N} & c_{b_Mb_1} & \cdots & c_{b_Mb_M} \\ \Delta s_{a_1} & \cdots & \Delta s_{a_N} & 0 & \cdots & 0 \\ 0 & \cdots & 0 & \Delta s_{b_1} & \cdots & \Delta s_{b_M} \end{pmatrix} \begin{pmatrix} \gamma_{a_1} \\ \vdots \\ \gamma_{a_N} \\ \gamma_{b_1} \\ \vdots \\ \gamma_{b_M} \end{pmatrix}}_{\begin{pmatrix} AA & AB \\ BA & BB \\ \Delta s_A & 0 \\ 0 & \Delta s_B \end{pmatrix} \begin{pmatrix} \gamma_A \\ \gamma_B \end{pmatrix}} = \underbrace{\begin{pmatrix} \mathrm{RHS}_{a_1} \\ \vdots \\ \mathrm{RHS}_{a_N} \\ \mathrm{RHS}_{b_1} \\ \vdots \\ \mathrm{RHS}_{b_M} \\ \Gamma_{\gamma,a} \\ \Gamma_{\gamma,b} \end{pmatrix}}_{\begin{pmatrix} \mathrm{RHS}_a \\ \mathrm{RHS}_b \\ \Gamma_{\gamma,a} \\ \Gamma_{\gamma,b} \end{pmatrix}} \tag{2.62}$$

where the diagonal matrices (AA, BB) are the self-induction matrix of the panel body and the non-diagonal terms (AB, BA) are the inter-induction matrix containing the panel influence of $B \rightarrow A$ and $A \rightarrow B$ respectively. The final two rows of the induction matrix contains the additional circulation constraint for each body.

2.4.3 Convergence study of panel method

The validation of the panel method was done by performing a convergence study of a cylinder. The vortex panels where used to simulate a potential flow around a cylinder and the solution of the panels was compared with the analytical solutions.

To test the solution of the vortex panels with the analytical solution, the problem was first run for the parameters in the table 2.1. The velocity field of the potential flow solution is shown in figure 2.15. The figure shows the norm of the velocity, and we see that it shows the velocity field of a potential flow solution, with an infinitely thin boundary layer, stagnating to zero velocity inside the body.

The jagged velocity field around the surface of the cylinder is simply due to the sampling resolution of the field; For higher resolution, this will not be there. In order to determine the accuracy of the solution, the velocity field of the panel solution was compared with

Parameters	Value	Unit
R	1	$[m \cdot s^{-1}]$
$\mathbf{u}_\infty$	$[1, 0]$	$[m \cdot s^{-1}]$
N_{panels}	100	$[-]$

Table 2.1: Panel study parameters

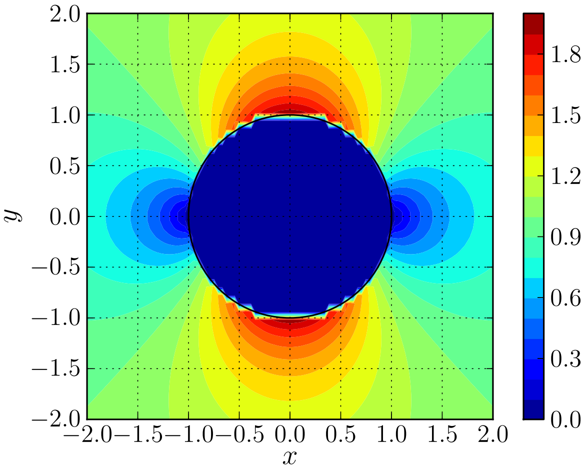

Figure 2.15: Panel method solution: Potential flow velocity field around unit cylinder. The figure depicts $\|\mathbf{u}\|$ with zero velocity inside the body.

the analytical solution. The analytical velocity field around a cylinder is given as,

$$u_r = u\left(1 - \frac{R^2}{r^2}\right)\cos\theta \tag{2.63a}$$

$$u_\theta = -u\left(1 + \frac{R^2}{r^2}\right)\cos\theta \tag{2.63b}$$

where u_r and u_θ are the radial and the angular velocity respectively. The equation 2.63 is a function of the radius from the center of the cylinder (in our case $r_0 = [0,0]$) and the radius of the cylinder R.

The velocity field of the panel was compared with this analytical solution along the y-axis from $y = 0$ to $y = 10$, figure 2.16a. Comparing the solutions of the plot we see that the solution of the vortex panels and the analytical potential flow solution matches everywhere except at the surface. This is correct because the potential flow solution has

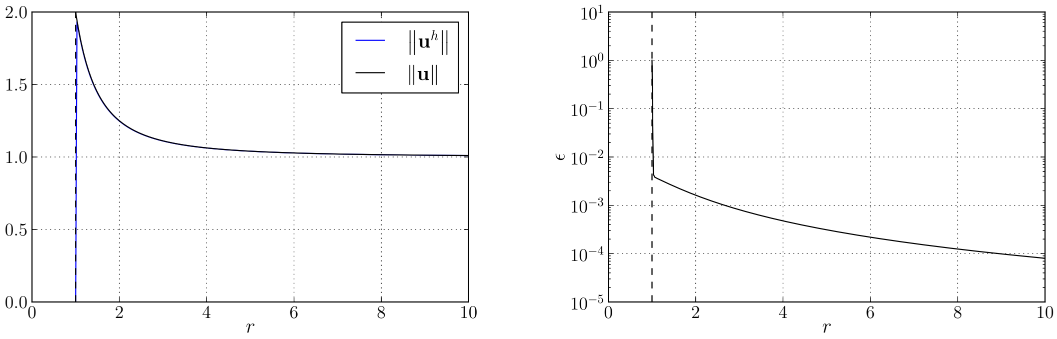

(a) Comparison of the velocity field.

(b) Error in velocity field

Figure 2.16: Comparison of the velocity field along the y-axis $0 \to 10$. Figure **(a)** shows both the solutions, the numerical $\|\mathbf{u}^h\|$ [solid blue,—] and the analytical solution [solid black, —]. Figure **(b)** shows the relative error ϵ between the solution, given by equation 2.64

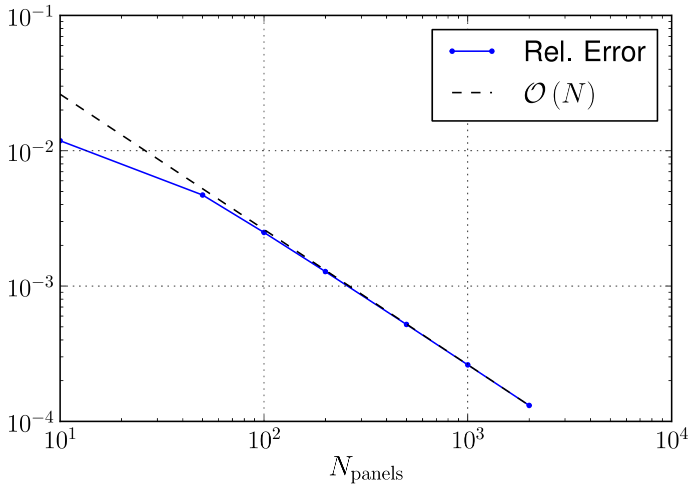

Figure 2.17: Convergence plot of the constant-strength straight vortex panels. The figures depicts the reduction is error at $\mathcal{O}(N)$.

a slip velocity (i.e non-zero velocity) at the surface of the body, whereas the vortex panels solves for a no-slip boundary condition at the collocation points of the surface. This explains the sudden drop of the velocity from two to zero at the surface.

The figure 2.16b shows the relative error ϵ between the numerical and the analytical solution,

$$\epsilon = \frac{\left\|\mathbf{u} - \mathbf{u}^h\right\|}{\|\mathbf{u}\|} \tag{2.64}$$

where $\mathbf{u}$ is the analytical solution and the $\mathbf{u}^h$ is the numerical (panel method) solution. Ignoring the solution right at the surface ($r = R$), we see that the error between the numerical and the analytical solution reduces from $\epsilon = 5 \times 10^{-3} \to 8 \times 10^{-5}$ as we go from $r = 1 \to 10$. This behavior of the error tells us that the solution of the constant-strength vortex panels gets more accurate as we go further away from the panels; right next to the panels, we have the largest error. This is because the vortex panels discretizes the body using a first-order approximation (straight panels) and also discretizes the vortex sheet strength using a first-order approximation.

The convergence analysis of the vortex panels shows that the panels that we are employing is indeed a first-order method as the error converges at $\mathcal{O}(N)$, figure 2.17.

2.5 Validation of lagrangian method

The validation of the lagrangian method was done by comparing the results of the Lamb-Oseen vortex and the analyzing the convection of the Clercx-Bruneau dipole. Validating each components of the hybrid method separately is vital as to ensure coupling is done correctly.

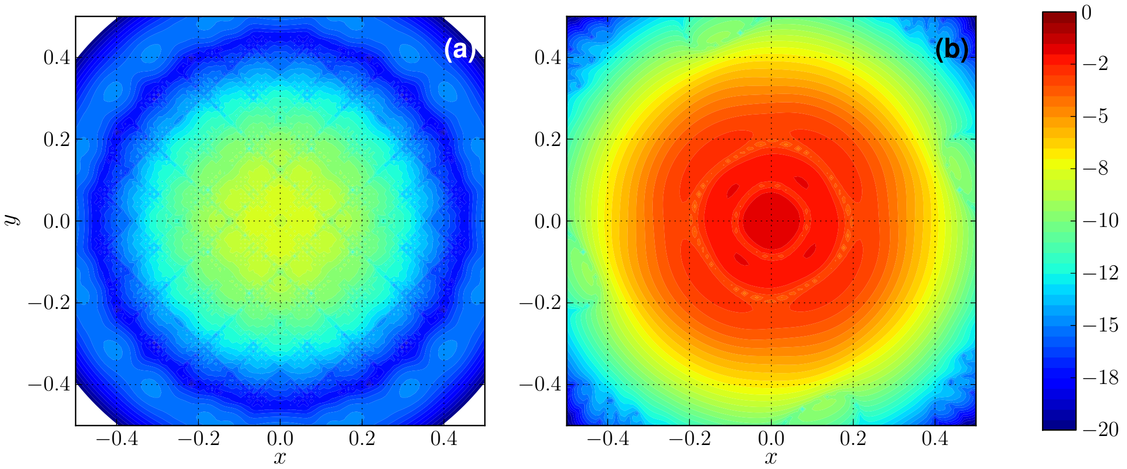

Figure 2.18: Error growth of Lamb-Oseen vortex during the evolution

2.5.1 Evolution of Lamb-Oseen vortex

The evolution of the Lamb-Oseen vortex can be considered to be one of the simplest to validate the viscous vortex method as it is derived from the diffusion equation.

2.5.2 Convergence study of the viscous vortex method

2.5.3 Convection of Clercx-Bruneau dipole at $Re = 625$

2.6 Summary

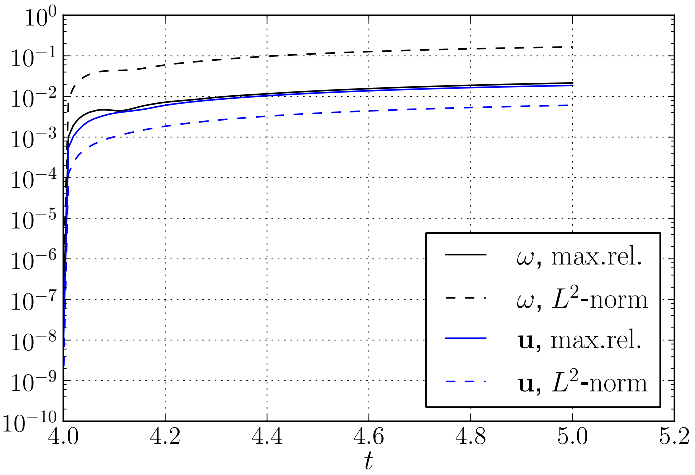

Figure 2.19: Error growth of Lamb-Oseen vortex during the evolution

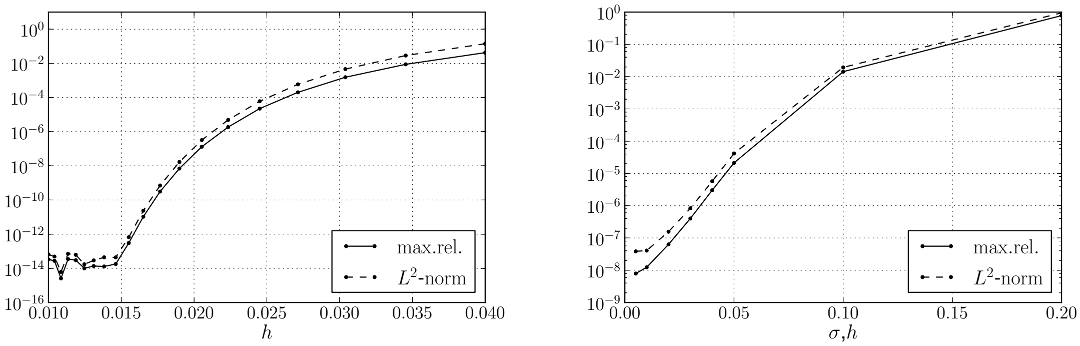

(a) Comparison of the velocity field.

(b) Error in velocity field

Figure 2.20: dx

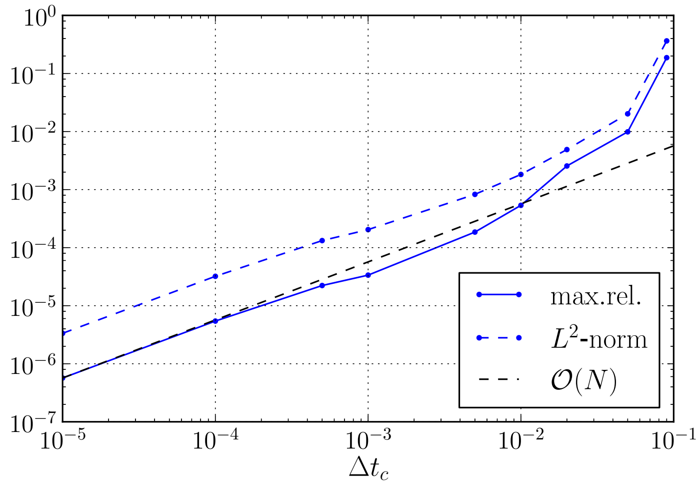

Figure 2.21: Error growth of Lamb-Oseen vortex during the evolution

Chapter 3

Eulerian Domain: Finite Element Method

3.1 Introduction to Finite Element Method

3.1.1 Finite element discretization

3.1.2 Finite element function and function space

3.2 Solving the Finite Element problem

3.2.1 Introduction to FEniCS Project

3.2.2 Mesh generation using GMSH

3.3 Solving Incompressible Navier-Stokes Equations

3.3.1 Velocity-pressure formulation

3.3.2 Incremental pressure correction scheme

3.3.3 Determining the vorticity field

3.3.4 Determining the body forces

Frictional Forces

Pressure Forces

3.4 Validation of eulerian method

3.4.1 Clercx-Bruneau dipole collison at $Re = 625$

3.4.2 Impulsively started cylinder at $Re = 550$

3.5 Summary

Chapter 4

Hybrid Eulerian-Lagrangian Vortex Particle Method

4.1 Theory of Domain Decomposition Method

4.1.1 Advantage of domain decomposition

4.1.2 Assumptions and Limitations

4.1.3 Modified coupling strategy

4.2 Eulerian-Lagrangian coupling algorithm

4.2.1 Eulerian dirichlet boundary condition

4.2.2 Vorticity interpolation algorithm

4.3 Introduction to pHyFlow: Hybrid solver

4.3.1 Program structure

4.4 Summary

Chapter 5

Verification and Validation of Hybrid Method

5.1 Error in coupling: Verification with Lamb-Ossen vortex

5.1.1 Generation of artificial vorticity

5.2 Clercx-Bruneau dipole convection at $Re = 625$

5.2.1 Comparison of vorticity contours

5.2.2 Variation in maximum vorticity

5.2.3 Variation in kinetic energy

5.2.4 Variation in enstrophy

5.3 Clercx-Bruneau dipole collison at $Re = 625$

5.3.1 Comparison of vorticity contours

5.3.2 Variation in maximum vorticity

5.3.3 Variation in kinetic energy

5.3.4 Variation in enstrophy

5.3.5 Variation in palinstrophy

5.4 Impulsively started cylinder problem at $Re = 550$

5.4.1 Evolution of the wake

5.4.2 Evolution of pressure and friction drag

5.4.3 Evolution of lift

5.5 Moving body

Chapter 6

Conclusion and Recommendation

6.1 Conclusion

6.1.1 Lagrangian domain

6.1.2 Eulerian domain

6.1.3 Hybrid method

6.2 Recommendations

6.2.1 Lagrangian domain

6.2.2 Eulerian domain

6.2.3 Hybrid method

References

[1] L.a. Barba and Louis F. Rossi. Global field interpolation for particle methods. *Journal of Computational Physics*, 229(4):1292–1310, February 2010.

[2] J.Thomas Beale. On the Accuracy of Vortex Methods at Large Times. In Bjorn Engquist, Andrew Majda, and Mitchell Luskin, editors, *Computational Fluid Dynamics and Reacting Gas Flows SE - 2*, volume 12 of *The IMA Volumes in Mathematics and Its Applications*, pages 19–32. Springer New York, 1988.

[3] AJ Chorin. Numerical study of slightly viscous flow. *Journal of Fluid Mechanics*, 1973.

[4] Christopher D Cooper, Santa Mar, and Lorena Barba. Panel-Free Boundary Conditions for Viscous Vortex Methods. *19th AIAA Computational Fluid Dynamics*, 2009(June):1–12, June 2009.

[5] G H Cottet and P D Koumoutsakos. *Vortex Methods: Theory and Practice*, volume 12. Cambridge University Press, 2000.

[6] G. Daeninck. *D EVELOPMENTS IN HYBRID APPROACHES Vortex method with known separation location Vortex method with near-wall Eulerian solver RANS-LES coupling*. PhD thesis, Universit catholique de Louvain, 2006.

[7] S. Degond, P.; Mas-Gallic, Pierre Degond, and S Mas-Gallic. The weighted particle method for convection-diffusion equations. I. The case of an isotropic viscosity. *Mathematics of Computation*, 53(188):485–507, 1989.

[8] C J Simão Ferreira, H Bijl, G Van Bussel, and G Van Kuik. Simulating Dynamic Stall in a 2D VAWT: Modeling strategy, verification and validation with Particle Image Velocimetry data. *Journal of Physics: Conference Series*, 75:012023, July 2007.

[9] CJ Simão Ferreira. The near wake of the VAWT: 2D and 3D views of the VAWT aerodynamics. 2009.

[10] JL Guermond and HZ Lu. A domain decomposition method for simulating advection dominated , external incompressible viscous flows. *Computers & fluids*, 29:525–546, 2000.

[11] Joseph Katz and A Plotkin. *Low-speed aerodynamics*. Cambridge Aerospace Series. Cambridge University Press, 2001.

[12] P Koumoutsakos. Inviscid axisymmetrization of an elliptical vortex. *Journal of Computational Physics*, 138(2):821–857, 1997.

[13] P Koumoutsakos, A Leonard, and F Pépin. Boundary Conditions for Viscous Vortex Methods. *Journal of Computational Physics*, 113(1):52–61, July 1994.

[14] PD Koumoutsakos. Direct numerical simulations of unsteady separated flows using vortex methods. 1993.

[15] J.J Monaghan. Extrapolating B-splines for interpolation. *Journal of Computational Physics*, 60(2):253–262, September 1985.

[16] ML Ould-Salihi, GH Cottet, and M El Hamraoui. Blending finite-difference and vortex methods for incompressible flow computations. *SIAM Journal on Scientific ...*, 22(5):1655–1674, 2001.

[17] S. Shankar and L.van Dommelen. A New Diffusion Procedure for Vortex Methods. *Journal of Computational Physics*, 127(1):88–109, August 1996.

[18] Doug Shiels. *Simulation of controlled bluff body flow with a viscous vortex method.* Dissertation (ph.d.), California Institute of Technology, 1998.

[19] Carlos Simão Ferreira, Gijs Kuik, Gerard Bussel, and Fulvio Scarano. Visualization by PIV of dynamic stall on a vertical axis wind turbine. *Experiments in Fluids*, 46(1):97–108, August 2008.

[20] Robert Speck. *Generalized algebraic kernels and multipole expansions for massively parallel vortex particle methods*, volume 7. Forschungszentrum Jülich, 2011.

[21] MJ Stock, A Gharakhani, and CP Stone. Modeling Rotor Wakes with a Hybrid OVERFLOW-Vortex Method on a GPU Cluster. *AIAA Applied Aerodynamics ...*, pages 1–12, 2010.

[22] O.R. Tutty. A Simple Redistribution Vortex Method (with Accurate Body Forces). *ArXiv e-prints*, September 2010.

[23] L.J. Vermeer, J.N. Sø rensen, and a. Crespo. Wind turbine wake aerodynamics. *Progress in Aerospace Sciences*, 39(6-7):467–510, August 2003.

[24] Daehyun Wee and Ahmed F. Ghoniem. Modified interpolation kernels for treating diffusion and remeshing in vortex methods. *Journal of Computational Physics*, 213(1):239–263, March 2006.

[25] Wikipedia. Vertical-Axis Wind Turbine, July 2013.

[26] G S Winckelmans, J K Salmon, Universite Catholique De Louvain, M S Warren, A Leonard, Theoretical Astrophysics, Los Alamos National Laboratories, Los Alamos, B Jodoin, and Universite De Sherbrooke. Application of Fast Parallel and Sequential Tree Codes to Computing Three-Dimensional Flows with the Vortex Element and Boundary Element Methods. 1:225–240, 1996.

[27] Grégoire Winckelmans, Roger Cocle, Louis Dufresne, and Raphaël Capart. Vortex methods and their application to trailing wake vortex simulations. *Comptes Rendus Physique*, 6(4-5):467–486, May 2005.